Blue-UV-Emitting ZnSe(Dot)/ZnS(Rod) Core/Shell Nanocrystals Prepared from CdSe/CdS Nanocrystals by Sequential Cation Exchange

Hongbo Li,[†] Rosaria Brescia,[†] Roman Krahne,[†] Giovanni Bertoni,[†,‡] Marcelo J. P. Alcocer,[§,⊥] Cosimo D'Andrea,[§,⊥] Francesco Scotognella,[⊥] Francesco Tassone,[§] Marco Zanella,[†] Milena De Giorgi,[∥] and Liberato Manna[†,*]

[†]Istituto Italiano di Tecnologia, via Morego 30, 16163 Genova, Italy, [‡]IMEM-CNR, Parco Area delle Scienze 37/A, 43124 Parma, Italy, [§]CNST of IIT@polimi, Via Pascoli 70/3, 20133 Milano, Italy, [⊥]Department of Physics, Politecnico di Milano, Piazza L. Da Vinci 32, 20133 Milano, Italy, and [∥]National Nanotechnology Laboratory of CNR-NANO, via per Arnesano km 5, 73100 Lecce, Italy

ABSTRACT Great control over size, shape and optical properties is now possible in colloidal Cd-based nanocrystals, which has paved the way for many fundamental studies and applications. One popular example of such class of nanocrystals is represented by CdSe(spherical core)/CdS(rod shell) nanorods. These can be nearly monodisperse in size and shape and have strong and stable photoluminescence that is tunable in the visible range (mainly by varying the size of the CdSe core). The corresponding Zn-based core/shell nanorods would be good candidates for tunable emission in the blue-UV region. However, while the synthesis of ZnS nanocrystals with elongated shapes has been demonstrated based on the oriented-attachment mechanism, elongated ZnS shells are difficult to fabricate because the more common cubic phase of ZnS has a highly symmetric crystal structure. We report here a procedure based on a sequence of two cation exchange reactions, namely, $Cd^{2+} \Longrightarrow Cu^{+}$ and then $Cu^{+} \Longrightarrow Zn^{2+}$, by which we transform colloidal CdSe(core)/CdS(shell) nanorods first into into Cu_2Se/Cu_2S nanorods, which are then converted into blue-UV fluorescent ZnSe(core)/ZnS(shell) nanorods. The procedure transfers the morphological and structural information of the initial Cd-based nanorods to the Zn-based nanorods. Therefore, the final nanoparticles are made by a ZnSe dot embedded in a rod-shaped shell of wurtzite ZnS. Since in the starting Cd-based nanorods the size of the CdSe core and the length of the CdS shell can be well controlled, the same holds for the final Zn-based rods. In the second step of the exchange reaction ($Cu^{+} \Longrightarrow Zn^{2+}$), a large excess of Zn^{2+} ions added over the Cu^{+} ions present in the Cu_2Se/Cu_2S nanorods is the key requisite to obtain bright, band-edge emission (with quantum yields approaching 15%) with narrow line widths (approaching 75 meV). In these ZnSe/ZnS nanorods, photogenerated carriers appear to be more confined in the core region compared to their parent CdSe/CdS nanorods.

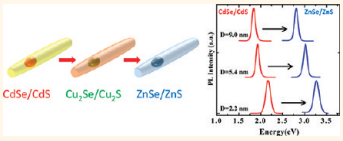

KEYWORDS: cation exchange · nanocrystals · nanorods · core/shell · ZnSe/ZnS

Colloidal ZnSe nanocrystals have received increasing attention during the last several years as a potential alternative to the more toxic Cd-based nanocrystals.[1−3] Research in this direction, besides achieving nanocrystals with controllable size and with narrow size distributions, has tackled various aspects, such as (i) doping, so as to shift their emission in the visible range of the spectrum,[2,4−6] (ii) shape control,[2,7] (iii) improving stability against surface oxidation and increasing at the same time the photoluminescence (PL) quantum yield (QY) by growing a shell of a higher band gap material around the starting nanocrystals,[8−14] (iv) in some cases several issues at once have been addressed, for example, doping and shell growth.[15] So far, stable blue-UV emission from colloidal nanocrystals has been achieved mainly *via* semiconductor alloy and/or core/shell nanocrystals or even *via* magic size clusters. However, in almost all cases, these nanocrystals contained cadmium.[16−23]

In the last year, new developments in the synthesis of ZnSe nanocrystals have come from cation exchange (CE) reactions. CE in nanocrystals of ionic materials has allowed the development of new types of nanostructures[24,25] and new applications that exploit this type of reaction in nanoparticles.[26−29] Usually, in CE, the framework of anions remains in place, while the cations can be partially or totally replaced by cations of another element.[24−27] One elegant demonstration of the anion framework conservation was recently given by Jain *et al.* on the transformation of colloidal CdSe(spherical core)/CdS(rod shell) nanorods (NRs) into the corresponding Cu_2Se(spherical core)/Cu_2S(rod shell) particles,[25] which proved that no interdiffusion of S and Se species occurred during the replacement of Cd^{2+} ions with Cu^{+} ions. Jain *et al.* also reported sequential CE reactions starting from CdSe/CdS NRs, involving a $Cd^{2+} \Longrightarrow Cu^{+} \Longrightarrow Pb^{2+}$ sequence of CE steps, again proving anion framework conservation.[25] Also, in another work of Jain *et al.*, it was shown that a cyclic reaction,

* Address correspondence to liberato.manna@iit.it.

Received for review November 26, 2011 and accepted January 20, 2012.

Published online January 27, 2012
10.1021/nn204601n

which started from CdSe/CdS nanocrystals, converted them into Cu_2Se/Cu_2S nanocrystals, and then back to CdSe/CdS ones, resulted in particles with much lower QY than in the starting sample.[30] The reason for this low QY was shown to be the residual presence of Cu ions in the lattice (below the detection limit of standard elemental analysis techniques), which the authors were able to extract, so that the QY could be restored to large values.

As another development in the field, our group recently demonstrated the conversion of CdSe nanocrystals of a given size, shape (either spherical or rod-shaped), and crystal structure (either hexagonal wurtzite or cubic sphalerite) into ZnSe nanocrystals by means of a sequence of two CE reactions: in the first step Cd^{2+} was replaced by Cu^+, then in the second step Cu^+ was replaced by Zn^{2+}.[31] A key aspect of the work was that the intermediate copper selenide nanocrystals were able to transfer all of the morphological and structural information of the initial CdSe nanocrystals to the final ZnSe ones.[31] Size and shape conservation in CE reactions is therefore an aspect that has been well-established and certainly can be exploited to develop nanostructures that are presently inaccessible by direct synthesis. Building on our previous work[31] and on that of Jain *et al.*,[25] we report here a procedure based on two CE reactions, by which we convert CdSe(spherical core)/CdS(rod shell) NRs into ZnSe(spherical core)/ZnS(rod shell) NRs, which likewise is able to transfer all of the morphological and structural information of the Cd-based NRs to the final Zn-based NRs (see Scheme 1). These Zn-based NRs are made therefore of a wurtzite ZnSe spherical dot embedded in a rod-shaped shell of wurtzite ZnS.

One important achievement of the present procedure stands in the correct identification of a suitable set of experimental conditions for the second CE step that yield NRs emitting from ZnSe band-edge states, with PL characterized by a narrow spectrum and appreciable QY (from 5 to 15%) and free from trap state emission. The PL emission of these NRs is narrower than that of other colloidal ZnSe and ZnSe/ZnS nanocrystals reported so far, and practically equal to that of the starting CdSe/CdS NRs. We studied the shifts of absorption and PL peak positions of core/shell NRs with respect to the same optical features of their nanocrystal seeds for a series of CdSe/CdS NRs of varying CdSe core sizes and for the corresponding series of ZnSe/ZnS NRs. The comparison between the two sets of data suggested that for the ZnSe/ZnS NRs photogenerated carriers appear to be more confined in the core region than for their parent CdSe/CdS NRs. We correlated these data with calculations based on the effective mass approximation, by which we could estimate a conduction band offset between ZnSe and ZnS equal to −350 meV, corresponding to an overall type I band alignment between ZnSe and ZnS.

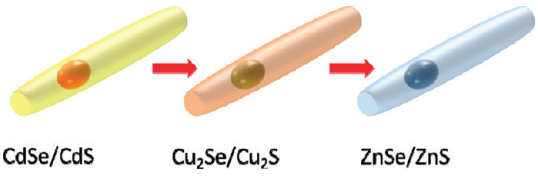

Scheme 1. Sequence of two CE reactions starting from CdSe(spherical core)/CdS(rod shell) NRs, going through Cu_2Se(spherical core)/Cu_2S(rod shell) NRs (as already described by Jain *et al.*[25]) and finally yielding ZnSe(spherical core)/ZnS(rod shell) NRs.

RESULTS AND DISCUSSION

Synthesis and Steady-State Optical Characterization. The starting CdSe/CdS NRs were prepared according to a procedure developed by us some years ago, with minor modifications.[32,33] We synthesized NRs starting from roughly spherical CdSe seeds of various diameters on which we grew rod-shaped CdS shells of various lengths. The first CE step ($Cd^{2+} \rightleftharpoons Cu^+$) was performed according to the procedure described by Jain *et al.*,[25] while the second CE step ($Cu^+ \rightleftharpoons Zn^{2+}$) was carried out following our recently reported approach to convert CdSe nanocrystals into ZnSe ones, in both cases with modifications.[31] Worthy of note is that the second step was carried out in the presence of trioctylphosphine at high temperature (250 °C) and working with a large excess of Zn^{2+} ions added over the total amount of Cu^+ ions present in the Cu_2Se/Cu_2S nanorods (over 100:1). These unique reaction conditions allowed massive extraction of the Cu^+ ions from the lattice and their replacement with Zn^{2+} ions. For both steps, the CE reactions were completed in a few seconds.[33] In Figure 1, the results of the exchange reactions starting from a representative sample of CdSe/CdS core/shell NRs are reported. For this sample, the starting NRs had a spherical CdSe core of 5.4(±0.5) nm in diameter that was covered with a 33(±3) nm long rod-shaped CdS shell. As can be seen from the sequence of transmission electron microscopy (TEM) images in Figure 1a−c, the shapes and sizes of the NRs were not changed after each CE reaction. However, a 7−8% contraction in the overall size in the final ZnSe/ZnS nanorods with respect to the parent CdSe/CdS ones is expected due to the contraction in the lattice parameters when going from CdS to ZnS and from CdSe to ZnSe. This change in size was generally not appreciable as it is smaller than the size dispersion of the particles, but a ~8% size contraction could be estimated when the largest CdSe seeds (8−9 nm in diameter) were converted into ZnSe seeds, which is ascribable to contraction in lattice parameters. This is an indication that there was no significant etching of the nanocrystals surface upon CE, which would have reduced their size further.

The optical features of the starting, intermediate, and final samples are reported in Figure 1d−f. Worthy of note is that the PL full width at half-maximum

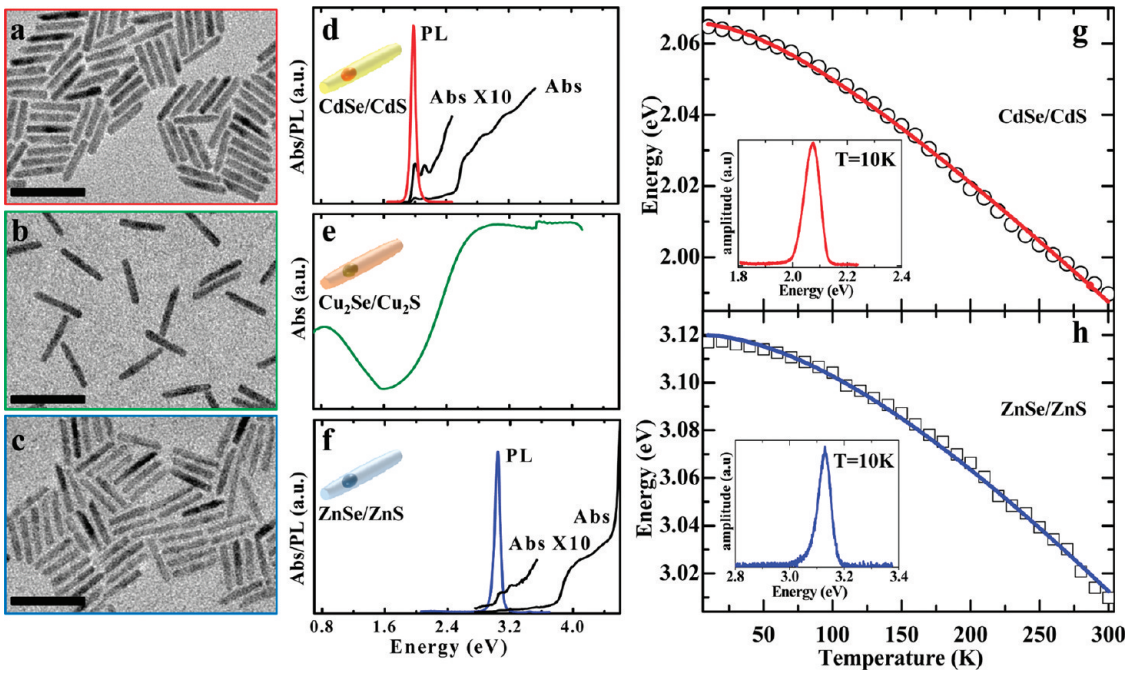

Figure 1. TEM images (a–c) and corresponding room temperature optical absorption and PL spectra (d–f) of the starting core/shell CdSe/CdS NRs with 5.4 nm CdSe cores and 33 nm long rod-shaped CdS shell (a,d) and of the corresponding Cu_2Se/Cu_2S NRs (b, e) (only absorption) and ZnSe/ZnS NRs (c,f) obtained *via* the CE reactions. The optical spectra varied drastically after each CE step, while the morphology and size of the NRs remained unchanged. The scale bars in the TEM images correspond to 50 nm. (g) Temperature dependence of the PL peak position for the CdSe/CdS NR sample shown in (a), along with the Varshni fit. The inset displays the PL peak at 10 K; (h) same optical data and fit as in (g) for the corresponding sample of ZnSe/ZnS NRs shown in (c).

(FWHM) of the starting Cd-based NRs (around 75 meV in this case) is conserved in the final Zn-based NRs, which suggests that the size monodispersity of the CdSe cores in the CdSe/CdS NRs is not altered when they are converted into ZnSe in the ZnSe/ZnS NRs. Also, the FWHM of the PL peak in these samples is much narrower than that of various colloidal ZnSe[34] and ZnSe/ZnS core/shell nanocrystals reported by other groups that were obtained by direct synthesis: for example, a peak FWHM of 162 meV (*i.e.*, 20 nm) was measured by Lomascolo *et al.* on colloidal spherical core/shell ZnSe/ZnS nanocrystals.[10] In the intermediate Cu_2Se/Cu_2S NRs, no PL was observed, but on the other hand, the optical absorption showed the emergence of a band around 0.8 eV that is plasmonic in origin[35–38] and that might be ascribed to the transverse plasmon mode in these NRs.

By increasing the temperature from 10 to 300 K, the photoluminescence spectra collected for both CdSe/CdS NRs and ZnSe/ZnS NRs exhibited a red shift of the PL peaks that followed the Varshni equation describing the temperature dependence of the semiconductor band gap.[39] Figure 1g,h displays such trends for one of the CdSe/CdS NR samples and for the corresponding ZnSe/ZnS sample obtained from it by CE (insets show PL spectra recorded at a temperature of 10 K). The Debye temperatures of the fits are characteristic of bulk CdSe (150 K) for the CdSe/CdS NRs and of bulk ZnSe (340 K) for the ZnSe/ZnS NRs, which indicates that radiative recombination in both cases occurred primarily from the core regions in the rods (the various parameters are given in the Supporting Information).

Structural and Compositional Characterization. We carried out extensive structural characterization of the ZnSe/ZnS NRs. Their X-ray diffraction (XRD) pattern, reported in Figure 2a for the sample shown in Figure 1c, matches well with that of the hexagonal wurtzite phase of ZnS. Clearly, as the volume fraction from the ZnSe cores in this sample is 10% of that of the whole rod (or even lower), the peaks from the wurtzite ZnSe phase are practically undetected. High-resolution TEM (HRTEM) confirms that in all of the NRs the ZnS shell is in the wurtzite phase (Figure 2b). The preservation of the wurtzite crystal phase of the shell of the initial CdSe/CdS NRs, after the conversion to ZnSe/ZnS, is consistent with our previous results on CE that started from wurtzite CdSe nanocrystals (either spherical or rod-shaped) and yielded wurtzite ZnSe nanocrystals.[31] In that case, as well as in the present case, the intermediate Cu-based rods have also hexagonal crystal structure, which ensures the transfer of phase information from the Cd-based rods to the Zn-based ones.

The wurtzite phase for ZnS and for ZnSe is metastable at room temperature (in ZnS, for example, the phase transition temperature from fcc to hcp is 1296 K),[40] and indeed in most cases, nanocrystals of these materials have been grown in the cubic sphalerite phase.[41] Up to now, only in a few reports nanocrystals of ZnSe and ZnS with hexagonal crystal structure were synthesized at relatively low reaction temperature.[3,40,42–47]

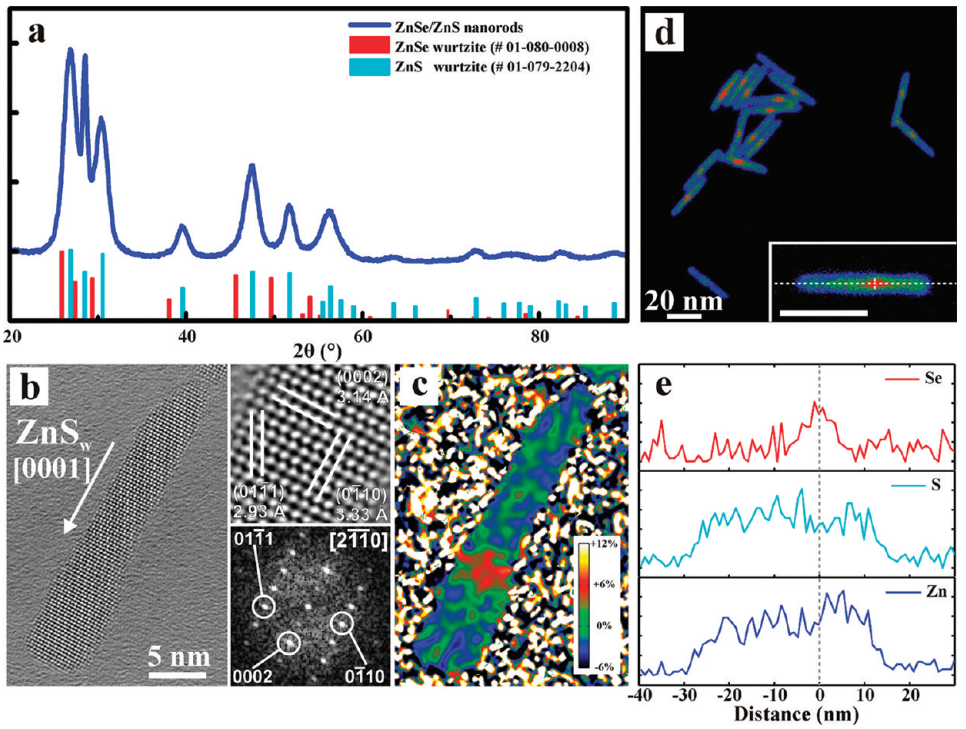

Figure 2. (a) XRD pattern of the ZnSe/ZnS NRs shown in Figure 1c; (b) HRTEM image and corresponding fast Fourier transform of a ZnSe/ZnS NR of the same sample, with indication of the lattice planes of wurtzite ZnS (ZnS_w); (c) mean dilation map of a single ZnSe/ZnS NR obtained *via* peak pairs analysis (PPA). An area with a mean dilation of 3.6(±0.9)% (red-yellow) with respect to unstrained ZnS (green-blue) can be seen in the central region of the rod, which can be justified by the presence of the ZnSe core; (d) false color image from a HAADF-STEM image of a group of ZnSe/ZnS NRs. Inset: Higher magnification of a NR. The dashed line indicates the scan direction for the EDS profiles; (e) EDS profiles of Se (L edge), S (K edge), and Zn (K edge) across the NR displayed in the inset in (d). The region of the particle showing the highest intensity (red) in HAADF-STEM is thus referable to the ZnSe core (the 0 in the EDS line scan corresponds to the cross in the inset).

ZnS has been used extensively as a material for the inorganic passivation shell in various type I core/shell nanocrystals.[42] Yet, while the synthesis of ZnS with elongated shapes has been demonstrated based on the oriented-attachment mechanism,[48,49] elongated ZnS shells are difficult to fabricate because of the more stable cubic phase of ZnS.

The analysis of HRTEM images of several ZnSe/ZnS NRs using the peak pairs algorithm, which maps the strain inside individual nanoparticles, allowed us to distinguish a region with a mean dilation of 3.9(±0.9)% with respect to the unstrained regions of the wurtzite ZnS shell at the two ends of each particle (Figure 2c and Figure S4 of the Supporting Information).[50,51] This strained region corresponds to the ZnSe core, as the dilation is compatible with the 4% lattice mismatch between bulk wurtzite ZnSe and wurtzite ZnS. At the same time, a region with higher contrast is identified roughly at the center of each rod by high-angle annular dark-field scanning TEM (HAADF-STEM), due to the atomic number contrast sensitivity ($\sim Z^2$) of this technique and to the higher atomic number of Se ($Z = 34$) with respect to S ($Z = 16$) (Figure 2d). Compositional mapping of individual rods, carried out *via* energy-dispersive X-ray spectroscopy (EDS) line scans on single rods, shows that the higher contrast regions in the rods are indeed referable to the ZnSe cores buried inside the ZnS shell (Figure 2e).

Several samples of ZnSe/ZnS NRs of varying core size and shell length/thickness were prepared starting from the appropriate CdSe/CdS NRs, and elemental analysis on all of the samples by inductively coupled plasma optical emission spectroscopy (ICP-OES) on digested solutions supported a complete conversion from CdSe/CdS NRs to Cu_2Se/Cu_2S NRs and from these to ZnSe/ZnS NRs (the concentration of Zn was around a few parts per million in our final ZnSe/ZnS NR samples and that of Cu was often close to the detection limit, which is around 10 ppb). We also performed elemental analysis on many particles by EDS, and likewise, we found a low content (comparable to or lower than the noise level) of both Cu and Cd in the final ZnSe/ZnS NRs (see Figure S3). The conversion yield is consistent with our former results on the synthesis of ZnSe nanocrystals.[31] Also, the S/Se molar ratio in the rods, as determined by elemental analysis, remained constant after each CE reaction and equal to that of the starting CdSe/CdS NRs,[33] indicating that no substantial amounts of S ions, neither of Se ions, were expelled from the particles.

A strong indication of the overall preservation of the Se/S anion sublattice in the NRs following CE was

given by the following experiment: we prepared first ZnSe/ZnS NRs as described above. Then we reconverted this sample into CdSe/CdS NRs by two reverse CE steps, namely, $Zn^{2+} \Rightarrow Cu^{+}$ followed by $Cu^{+} \Rightarrow Cd^{2+}$.[33] The morphology of these final rods was the same as that of the initial sample. Also, the optical absorption and emission spectra of the final CdSe/CdS NRs were comparable to those of the initial CdSe/CdS NRs (see Figure 3), with the PL of the final sample exhibiting only a spectral shift in the blue of about 20 meV (and a 75% loss in QY) with respect to the PL of the initial sample. If, in any of the four steps involved in this cyclic process, the Se/S anion framework had been disturbed considerably, this should have resulted in a substantial alloying between core and shell. Then, we should have observed a much stronger blue shift than what we actually found experimentally.

Quantum Yield (QY) and Stability over Time. The QY of the ZnSe/ZnS NRs was measured by using aminopyridine as a reference dye.[33] The highest QY (15%) was measured on a NR sample with a ZnSe core size of 5.0 nm. Apparently, samples with core sizes either smaller or larger than 5.0 nm had lower QYs. We measured for example 12% in the case of 2.1 nm ZnSe core size and 6% in the case of 8.4 nm ZnSe core size. For a given core size, we found that two parameters play a key role in determining the QY, namely, the ratio of Zn^{2+} ions added to the total amount of Cu^{+} ions present in the intermediate Cu_2Se/Cu_2S NRs and the temperature at which the $Cu^{+} \Rightarrow Zn^{2+}$ exchange was carried out. The highest values of QYs (*i.e.*, those reported above) were found for Zn/Cu ratios above 100 and temperatures above 200 °C. With regard to the Zn/Cu ratio, large excess of Zn^{2+} ions should ensure quantitative extraction of Cu ions from the lattice. Also, high temperatures should help to extract Cu ions and in general to anneal defects. Unfortunately, with the present synthesis scheme, we could not go to temperatures beyond 250 °C as the NRs started undergoing a change in shape.

Reactions carried out when either one or both parameters (Zn/Cu ratios, temperature) were below those thresholds yielded samples with much lower QYs. When the Zn/Cu ratio was below 50, the samples exhibited significant trap emission (Figure S1).[33] One possible source of defects in the NRs obtained at lower Zn/Cu ratio could be the presence of residual copper in the lattice. The concentration of copper in the final, cleaned ZnSe/ZnS NRs, as assessed by elemental analysis (*via* both ICP-OES and EDS; see above and Figure S3), was close to the detection limit. However, even a few Cu ions left per particle are expected to influence considerably the optical behavior, as pointed out in the recent work by Jain *et al.* on CdSe/CdS nanocrystals.[30] In addition to that, lattice vacancies formed during the CE reaction may also be responsible for trap emission. In our case, we can rule out the strain

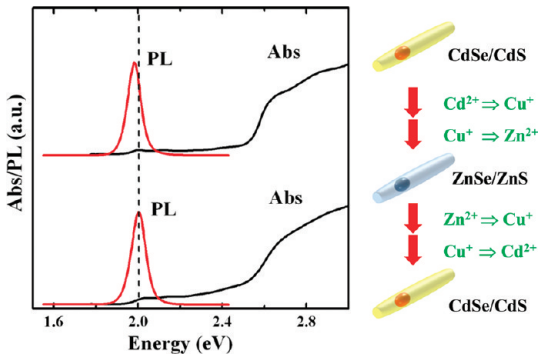

Figure 3. Optical absorption and emission spectra of an initial sample of CdSe/CdS NRs (top) and corresponding spectra after the sample was converted to ZnSe/ZnS NRs and back to CdSe/CdS NRs (bottom). The PL of the final sample was blue-shifted by about 20 meV (and had a 75% loss in QY) with respect to the PL of the initial sample. The data suggest an overall preservation of the Se/S anion sublattice in the NRs following CE.

at the ZnSe/ZnS interface as a major cause of low QY since such strain is comparable to that at the CdSe/CdS interface in CdSe/CdS nanocrystals, yet in these latter samples large QYs are usually observed.

The QYs from the present ZnSe/ZnS NRs are certainly lower than those of their parent CdSe/CdS NRs (30−50%), but they are not too far from the values reported on core/shell ZnSe/ZnS nanocrystals synthesized using more traditional methods.[45] For instance, the bare ZnSe nanocrystals reported by Chen *et al.* had QYs around 6−10%,[45] which went up to 32% after growth of a ZnS shell. The highest reported QY values for core/shell ZnSe/ZnS nanocrystals are in any case always lower than 50% (45% in Dong *et al.*,[52] 9% in Aboulaich *et al.*[53]). On the other hand, up to now, only a few synthesis routes have been able to produce highly fluorescent nanocrystals using CE reactions, one notable example being the one related to the synthesis of colloidal $Hg_xCd_{1-x}Te$ quantum dots,[54] while in most cases the QY of the nanocrystals was very low (*i.e.*, below 1%). Possible reasons for such low optical quality might be related to the fact that CE reactions can induce as a side effect the formation of a large number of crystal defects, including residual ions as stated above.[30] Another important example of particles exhibiting strong fluorescence after CE is represented by PbSe/CdSe nanocrystals.[55] Here, the fluorescent PbSe core is actually not affected by the CE reaction, which only involves the formation of a CdSe shell. This, together with other parameters (low lattice mismatch at the interface, slow chemical reaction), is likely to be responsible for the preservation (and actually improvement) of the PL QY, compared to other nanocrystal systems subjected to CE.

The optical stability of our ZnSe/ZnS NRs was greatly enhanced with respect to that of the bare ZnSe nanocrystals (which are strongly sensitive to oxygen and lose their PL in a few minutes) but was nonetheless

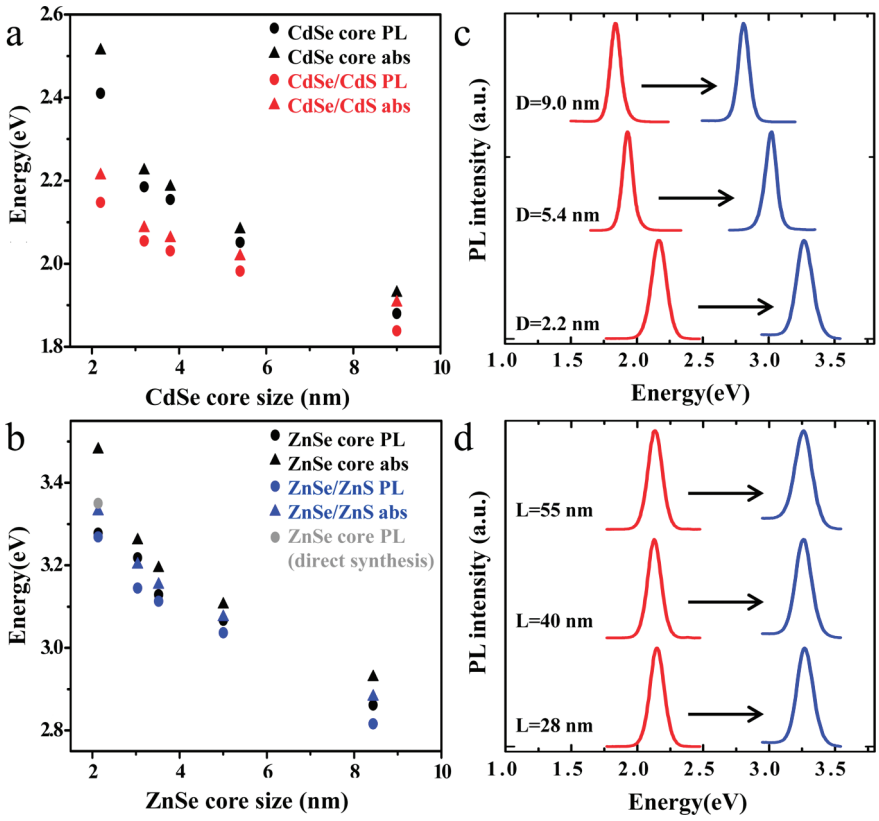

Figure 4. (a) Energy of the lowest energy peak in the optical absorption (▲) and of the PL peak (●) from samples of spherical CdSe nanocrystals of various diameters (CdSe core size) and corresponding optical data (red triangle = absorption, red dot = PL) from samples of core/shell CdSe/CdS NRs synthesized using those CdSe nanocrystals as seeds. (b) Optical data for the corresponding samples of spherical ZnSe nanocrystals (black triangle = absorption, black dot = PL) and core/shell ZnSe/ZnS NRs (blue triangle = absorption, blue dot = PL) obtained from the various samples of panel (a) by cation exchange. In the case of the small spherical ZnSe nanocrystals (2.1 nm in diameter), their synthesis *via* cation exchange from CdSe yields unstable seeds, which tend to cluster together; therefore, their PL tends to shift to lower energy than for well-dispersed nanoparticles. For a comparison, we report then with the gray solid dot the PL of a sample of sphalerite ZnSe nanocrystals obtained by direct chemical synthesis (see ref 7) and whose lowest energy peak in the optical absorption matches that of the 2.1 nm ZnSe nanoparticles obtained by CE; (c,d) display how the PL spectra evolve when transforming various samples of CdSe/CdS NRs to ZnSe/ZnS NRs. In (c), a series of CdSe/CdS NRs with a different core diameter (*D*) and the same rod length (*L* = 33 nm) were transformed into ZnSe/ZnS NRs; in (d), the transformation concerns a series of CdSe/CdS NRs with the same core diameter (*D* = 2.2 nm) but different length *L*. In both CdSe/CdS NRs and ZnSe/ZnS NRs, the PL peak position is basically dictated by the core size.

lower than that of their parent CdSe/CdS NRs, which are known to be very stable. As an example, we monitored the QY of a sample of ZnSe/ZnS NRs left under air at room temperature for 3 days (Figure S2 of the Supporting Information). After exposure to air for 2 h, the QY dropped by about 35% (compared to the starting value) and by 57% after 3 days. This drop in QY was often accompanied by the emergence of a broad band at lower energies, due to trap emission. It is also likely that residual lattice defects (formed as a consequence of CE) can play an important role in undermining the optical stability of these NRs.

Evolution of Optical Spectra with Varying Core Size and Rod Length: Comparison of Zn-Based Nanocrystals with Their Parent Cd-Based Nanocrystals. In one set of experiments, we compared the optical properties of a series of ZnSe/ZnS NRs, characterized by comparable lengths (around 28−33 nm) but different ZnSe core diameters, with those of their parent CdSe/CdS NRs. As discussed above, it appears that the anion framework in all of the nanocrystals studied ensures that the size of the particles does not change significantly upon CE, but on the other hand, a 7−8% size reduction due to lattice contraction must be taken into account. Unfortunately, this could be hardly appreciated even in the case of the NRs with large seeds, due to their size dispersion. For the smallest seeds too, clearly there must be lattice contraction upon CE (for example, a 2.2 nm CdSe seed should be reduced to a 2.0 nm ZnSe seed), but this again could be hardly evaluated by TEM. In view of these difficulties in assessing small size variations in samples characterized by a non-negligible size distribution, we therefore decided to consider the sizes of the various ZnSe cores (or seeds) of all the Zn-based nanocrystals in Figure 4b and in Table 1 (values in parentheses) as simply equal to those of their parent Cd-based nanocrystals but reduced in size by 7%.

For the sake of clarity, we summarize first the trends related to the CdSe/CdS NRs and then we move on describing the Zn-based NRs. Figure 4a reports the

TABLE 1. Calculated Energies of the Optical Transitions in ZnSe Seeds and ZnSe/ZnS NRs as Functions of the Core Size, Which Is the Same as the Size of the Seeds[a]

core size [nm]	2.0 (2.1)	3.0 (3.0)	3.6 (3.5)	4.8 (5.0)
ZnSe seed [eV]	3.51 (3.48)	3.22 (3.26)	3.13 (3.19)	3.02 (3.10)
ZnSe/ZnS NRs [eV]	3.25 (3.33)	3.11 (3.20)	3.05 (3.15)	2.98 (3.07)

[a] Experimental values are shown in parentheses. The core size was slightly reduced in some of the calculations compared to the experimental values in order to better match the measured transition energies for the seeds. This reduction is slightly overvalued because we neglected the small hole confinement energy in the calculation of the optical transitions. However, these adjustments are relatively small, and their impact on the energy shifts is expected to be limited. In particular, the trend of the red shifts due to shell overgrowth with core size is well-reproduced. The transition energies of the NRs are systematically undervalued by about 80–100 meV. This might be ascribed to strain effects, as discussed later in the text.

spectral positions of the lowest energy absorption peak, called henceforth "absorption peak" (black triangles), and of the PL peak (black circles) for several samples of spherical CdSe nanocrystals of various diameters and for the CdSe/CdS NRs prepared from them, with 33 nm long CdS shells. All of the Cd-based samples (both the CdSe seeds and the CdSe/CdS NRs) were then cation-exchanged to the corresponding Zn-based nanocrystals, and their relevant optical data are reported in Figure 4b (triangles mark absorption, circles mark PL).

For the Cd-based nanocrystals (Figure 4a), the energy difference between their absorption peak (black triangles) and that of the CdSe/CdS NRs prepared from them (red triangles) widens with decreasing size of the CdSe seeds. A similar trend is observed for the PL peaks (compare black circles with red circles in the same figure). With decreasing seed size, both absorption and PL features of the core/shell NRs are increasingly red-shifted from those of their initial CdSe seeds. These shifts exceed 100 meV for seeds of 3.8 nm diameter and reach 300 meV for 2.2 nm seeds. This trend can be explained by quantum confinement: with decreasing CdSe seed size, there is a widening in the gap between electron and hole states in CdSe (the equivalent of the band gap in the bulk). Similar effects occur also for the states of the CdS shell, whose diameter decreases, too, but those are less striking. In addition, the band alignments for bulk CdSe and CdS are such that there is a large offset in valence band maxima (VBM) but small offsets between conduction band minima (CBM). Then, with decreasing size of the CdSe seed in core/shell NRs, there is a concomitant decrease in the energy offset between the lowest electron states in the CdSe core and the lowest electron states in the CdS shell. This causes an increasing delocalization of the electron wave function over the CdSe core into the CdS shell, even for the lowest exciton state, an aspect that was already pointed out in previous works.[32,56]

In the Zn-based nanocrystals (Figure 4b), the shifts between absorption peaks of the seeds (black triangles) and of their corresponding core/shell NRs (blue triangles) remained small, as they did not exceed 60 meV even for sizes down to 3.0 nm, which points in this case to a weak delocalization of the photoexcited carriers wave functions into the ZnS shell. Only for the sample of NRs with ZnSe cores around 2.1 nm the shift with respect to the seed was of 150 meV, indicating a more significant carrier delocalization. Comparison of the PL peaks (black and blue circles, respectively) for all of the samples of ZnSe seeds and corresponding ZnSe/ZnS NRs leads to similar conclusions. Here, however, the ZnSe seeds obtained from the 2.2 nm CdSe seeds were unstable and tended to cluster together, which is probably the reason why their PL was at much lower energy (3.28 eV) compared to that of their absorption peak (3.48 eV). We therefore indicate with a gray circle in Figure 4b the estimated PL peak position (3.35 eV) of a sample of spherical ZnSe nanocrystals prepared by direct chemical synthesis (see ref 7), whose absorption peak matches that of these "unstable" 2.1 nm ZnSe nanoparticles obtained *via* CE. These nanocrystals, however, had cubic sphalerite structure and not hexagonal structure; therefore, this data point must be considered with care. Summarizing, the overall data on Zn-based nanocrystals point to a type I band alignment between ZnSe and ZnS, hence to an almost complete confinement of carriers in the ZnSe cores, at least for core sizes down to 3 nm.

As one consideration on these optical data, it is clear that the shifts in energy discussed above depend also on the thickness of the CdS and ZnS shell in their respective core/shell NRs. Although such thickness remained more or less constant in the various core/shell NRs that we synthesized, we should consider that small variations in shell thickness from sample to sample will slightly affect the above-described picture on energy shifts for the two series of samples. The shifts should not depend strongly on the length of the CdS and ZnS shell. Panels c and d in Figure 4 show how the PL spectra evolve when transforming various representative samples of CdSe/CdS NRs to ZnSe/ZnS NRs. In Figure 4c, samples of CdSe/CdS NRs with different core size and the same length (33 nm) were transformed into ZnSe/ZnS NRs; in Figure 4d, the transformation concerns a series of CdSe/CdS NRs with the same core size (2.2 nm) but different lengths. In both CdSe/CdS NRs and ZnSe/ZnS NRs, the PL peak position is practically dictated only by the core size.

Theoretical Modeling and Comparison with Previous Works. For CdSe/CdS NRs, it is quite established both from experiments and from theoretical models that the overall band alignment between CdSe and CdS goes from type I to quasi-type II as the size of the CdSe cores shrinks below 2.8–3 nm.[56] For ZnSe/ZnS, this aspect has not been approached in detail so far from a theoretical point of view. Also, the comparison of our results on the optical behavior of wurtzite ZnSe/ZnS core/shell NRs with previous reports is not

straightforward since, in most of those works, the ZnSe/ZnS nanocrystals were in the sphalerite structure, while in the present case all domains are in the wurtzite structure. The only obvious analogy of our findings with previous reports is that a shell growth induces a small red shift in both the optical absorption and emission spectra.

One important question to start with is how the relative band alignment between bulk ZnSe and bulk ZnS changes when the phase of the two materials is hexagonal instead of cubic. In this respect, self-consistent pseudopotential calculations carried out by Northrup *et al.*[57] on the (111−0001) ZnS−ZnS and (111−0001) ZnSe−ZnSe sphalerite−wurtzite bulk interfaces can be instructive. It was found that the upward shift in energy in the conduction band of wurtzite ZnS for the (111−0001) ZnS−ZnS interface is higher than that of wurtzite ZnSe for the (111−0001) ZnSe−ZnSe interface. Then, from these calculations, one can infer that the conduction band offset (CBO) at a bulk wurtzite ZnSe/wurtzite ZnS interface is larger than the CBO at a bulk sphalerite ZnSe/sphalerite ZnS interface. Extrapolating to the present nanocrystal case, in samples of core/shell ZnSe/ZnS nanocrystals having the same core size and shell thickness but different crystal phase, electrons should be more confined in the core in the case of wurtzite core/shell nanocrystals than in the case of sphalerite core/shell nanocrystals.

In order to get more insight in the issue of the CBO and possible electron delocalization in the ZnS shell for ZnSe/ZnS NRs, we performed a calculation of the lowest electron wave function and confinement energies in ZnSe cores and ZnSe/ZnS NRs within the effective mass approximation, using the CBO as a parameter.[33] Transition energies were estimated by neglecting the hole confinement energies, which should be considerably smaller than electron confinement energies due to the large valence band offset and large carrier effective mass. The shell diameter was held fixed, 1 nm larger than the core, and the seed dimensions were slightly reduced in some cases to better match the experimental energies. A reasonable trend of the energy shifts of absorption with shell overgrowth could be obtained by considering a relatively large CBO of about −350 meV, as shown in Table 1.

Even with the large CBO of −350 meV estimated by us, in the case of small (around 2 nm) ZnSe cores, the calculated shifts between optical features of the cores and those of the core/shell NRs are larger than what we found experimentally. Such red shift of the electron energy upon growth of the shell for a small ZnSe core, even for relevant CBO, can be explained as due to the small electron effective mass and to quantum confinement. Indeed, the zero-point energy for strong confinement in the core becomes substantially larger than any reasonable CBO for cores of small diameter. Also, one important factor that we have neglected up to now is strain. Given the 4% lattice mismatch between ZnSe and ZnS, strain effects could additionally affect the CBO in core/shell nanocrystals, as highlighted recently by Smith *et al.*[58] *Ab initio* all-electron calculations of absolute volume deformation potentials in various semiconductors have shown that the shift of the bands due to deformation of the lattice is generally much stronger for the conduction band minimum than for the valence band maximum.[59] In our core/shell NRs, the ZnSe core is buried inside a rod-shaped ZnS shell that should likewise induce a compressive strain on the ZnSe cores, which is even larger than for the more traditional ZnSe/ZnS core/shell nanocrystals characterized in general by a thinner ZnS shells. This compressive strain on the ZnSe core increases the optical band gap and CBM of ZnSe, whereas the tensile strain on the ZnS shell should lower the gap and CBM of the shell, at least in the vicinity of the ZnSe core. Summarizing, both strain effects and quantum confinement should contribute to "spilling" of the electron wave functions in the ZnS shell, especially for ZnSe cores with diameters smaller than 3 nm.

PL Lifetime Measurements. We carried out PL lifetime measurements at room temperature for selected samples of both series of CdSe/CdS and ZnSe/ZnS NRs. Representative decay signals are displayed in the Supporting Information for ZnSe/ZnS NRs with small (2.3 nm) and large (5.0 nm) ZnSe cores (Figure S6). The PL decays could be fitted with a biexponential function for ZnSe/ZnS NRs and with a single exponential function for CdSe/CdS NRs. In ZnSe/ZnS NRs, the long (short) estimated decay times τ_l (τ_s) are around 3 (0.4) ns for the smaller dots of 2.1 and 2.3 nm and around 3.8 (0.3) ns for dots of 3.0 and 5.0 nm diameter. In all cases, the long time decay component yields a larger contribution to the integrated PL and therefore to QY. Given that the measured QYs are on the order of 12−15% for these samples, we may estimate the radiative lifetimes $\tau_r = \tau/\mathrm{QY}$ as being around 25 ns. These will be an overestimate as the short decay contributions have been ignored. For CdSe/CdS NRs, the lifetimes ranged from 15 to 30 ns, in accordance with previous works.[32,60−62] Taking into account the estimated QYs, radiative lifetimes are of the order of 50 ns, which are longer than those of ZnSe/ZnS NRs.

The relatively short radiative lifetimes in the ZnSe/ZnS NRs are consistent with good overlap of electron and hole wave functions and are therefore consistent with the considerations on the small red shifts by ZnS shell overgrowth reported above. We note that, even though the radiative lifetimes of CdSe/CdS NRs are longer (as also reported by She *et al.*[62]), the emission wavelength of these NRs is typically about 1.5 times longer than that of the ZnSe/ZnS NRs. Therefore, a radiative lifetime about 1.5 times larger is expected for similar overlap of the electron and hole wave functions

(as deduced from Fermi Golden Rule for radiative decay) and almost constant momentum matrix elements in direct gap semiconductors.[63,64] Thus, the radiative lifetimes found for these CdSe/CdS NRs are indicative only of rather *mild* electron wave function delocalization over the CdS rod, as instead a full delocalization would entail much longer radiative lifetimes. This observation might also explain the rapid saturation of the increase of radiative lifetime as a function of rod length found by She *et al.*[62]

CONCLUSIONS

In conclusion, we have reported the synthesis of ZnSe/ZnS NRs based on sequential cation exchange reactions, starting from CdSe/CdS NRs. These ZnSe/ZnS NRs preserve the morphological and structural features of their parent CdSe/CdS NRs (overall shape, anion Se/S framework, crystal structure) and in addition exhibit narrow PL spectra characterized by appreciable QYs. By combining optical studies with calculations, we could identify a stronger localization of the electron wave function in the ZnSe cores of the ZnSe/ZnS NRs than in the CdSe cores of CdSe/CdS NRs. The direct synthesis of anisotropic nanostructures based on ZnSe and ZnS is not straightforward, and therefore, our demonstration of rod-shaped ZnSe/ZnS nanocrystals obtained by cation exchange offers a solution in this direction.

EXPERIMENTAL SECTION

Synthesis of CdSe/CdS Core/Shell NRs. CdSe/CdS core/shell NRs were synthesized according to a published method developed by Carbone *et al.*[32] First, the CdSe seeds with different sizes were prepared by varying the injection temperature and the growth time. The obtained CdSe seeds were purified by repeated cleaning and then dispersed in trioctylphosphine (TOP). Second, the CdSe/CdS core/shell NRs were prepared *via* the seeded growth method by using the obtained CdSe seeds. The length of the final CdSe/CdS NRs could be tuned by varying the amount of sulfur precursor and of CdSe seeds. Additional details about the synthesis are reported in the Supporting Information. As a note, in this work, we describe the seeds (*i.e.*, the cores) in these core/shell NRs as spherical for the sake of simplicity, despite their real shape not being perfectly isotropic due to their crystalline nature, which leads to faceting and/or might also have slight elongations along certain crystallographic directions.

Synthesis of ZnSe/ZnS Core/Shell NRs *via* Cation Exchange Reactions. ZnSe/ZnS core/shell NRs were prepared *via* a sequence of two cation exchange reactions. In a standard procedure, the first cation exchange reaction, that is, from CdSe/CdS to Cu_2Se/Cu_2S, was performed following the protocol of Jain *et al.*,[25] which was also followed by us in a recent work of ours.[31] In a typical synthesis, a solution of Cu^+ cations was prepared by dissolving 10 mg (0.027 mmol) of $[Cu(CH_3CN)_4]PF_6$ into 1 mL of methanol. The CdSe/CdS NRs were dispersed in 5 mL of toluene (the solution contained 1 mg of CdSe/CdS NRs based on ICP data), and the resulting solution was mixed with the above $[Cu(CH_3CN)_4]PF_6$ solution. The atomic ratio of Cu/Cd was 3. The resulting mixture was kept at room temperature for 5 min and then was centrifuged at 3200 rpm to precipitate the Cu_2Se/Cu_2S NRs. After washing the samples with methanol and toluene two times, the obtained Cu_2Se/Cu_2S NRs were suspended in 2 mL of TOP, and the resulting solution was used as "injection solution" for the synthesis of ZnSe/ZnS NRs. The second cation exchange reaction, that is, from Cu_2Se/Cu_2S NRs to ZnSe/ZnS NRs, was performed as we described in our previous paper, with modifications.[31] A stock solution of Zn^{2+} cations was prepared by dissolving 2 mmol $ZnCl_2$ in a solution of 6 mL of degassed octadecene and 4 mL of degassed oleylamine at 250 °C under N_2 flow. The Cu_2Se/Cu_2S NRs obtained in the first step were injected into the Zn solution and kept in the hot solution for 5 min to complete the cation exchange reaction. After the synthesis, the ZnSe/ZnS NRs were precipitated with methanol; they were washed by repeated redissolution in toluene and precipitation with the addition of methanol and were finally dissolved in toluene.

Structural and Compositional Characterization. Overview TEM images were recorded on a JEOL JEM-1011 microscope operating at 100 kV. HRTEM, STEM-HAADF, and elemental analyses by EDS were performed using an ultra-high-resolution microscope (JEM-2200FS) with a field emission gun working at 200 kV, equipped with a CEOS image aberration corrector and a Si(Li) EDS detector. XRD measurements were performed with a Rigaku SmartLab X-ray diffractometer operating at 40 kV and 150 mA. The elemental analysis of the obtained particles was performed by using an ICP-OES spectrometer (iCAP 6500, Thermo).

Optical Characterization and QY. Absorption spectra were recorded with a Varian Cary 5000 UV−vis−NIR absorption spectrophotometer. In the case of Cu_2Se/Cu_2S NRs, these were dispersed in TCE, while toluene was used as solvent to disperse the CdSe/CdS NRs and hexane was used for the ZnSe/ZnS NRs. The fluorescence emission was collected using a CARY Eclipse (Varian) photoluminescence spectrometer. The PL QY of the ZnSe/ZnS NRs were measured by referencing to a standard (aminopyridine in 0.1 M H_2SO_4, QY = 60%) following a procedure reported in the literature.[65]

Temperature-Dependent PL Measurements. These were performed under vacuum (10^{-5} mbar) on NR films that were deposited onto Si substrates by drop-casting. The samples were mounted onto the cold head of a Janis closed cycle cryocooler coupled to a Lakeshore 336 temperature controller and illuminated by a Spectra Physics diode laser emitting at 350 nm that was coupled to an optical fiber. The pump power was of the order of 500 $\mu W/mm^2$. The signal was collected with a second fiber and analyzed by a Horiba-Jobin iHR320 spectrometer coupled to a Symphony CCD camera.

Time-Resolved PL (TRPL) Measurements. The TRPL measurements were performed using a femtosecond laser source and streak camera detection system. Pulses of approximately 140 fs in duration with central wavelengths around 740 nm for ZnSe/ZnS NRs and around 880 nm for CdSe/CdS NRs with a maximum energy of 50 nJ were produced by a tunable Ti:sapphire laser (Coherent Chameleon Ultra II) at a repetition rate of 80 MHz. A β-barium borate crystal was used for type I phase-matched second harmonic generation, leading to pulses with central wavelengths of 370 and 440 nm for ZnSe/ZnS and CdSe/CdS NRs, respectively. The collected emission was analyzed by a spectrograph (Princeton Instruments Acton SP2300) coupled to a streak camera (Hamamatsu C5680) yielding spectral resolution around 1 nm and temporal resolution dependent on the setup. In particular, for CdSe/CdS NRs, the repetition rate was reduced to 2 MHz by the use of an acousto-optical modulating pulse picker (APE Pulse Select), and the acquisition was obtained with linear voltage sweeping, achieving a maximum temporal resolution of about 50 ps. ZnSe/ZnS NRs were also measured at the 80 MHz repetition rate, leading to a maximum temporal resolution of ~3.6 ps. The optical density of the samples was checked to be well below 0.1 at the emission wavelength, and the excitation power was reduced to avoid saturation effects.

Calculations. The lowest electron wave functions and eigenvalues of a dot and a nanorod (NR) geometry were calculated within the effective mass approximation, that is, solving the

Schrödinger equation for the electron using a finite element method and considering different effective masses for the electron in the ZnSe seed (*i.e.*, the core) ($m_e = 0.13m_0$, with m_0 being the free electron mass) and the ZnS rod ($m_e = 0.21m_0$).[66] For the seed case, the external potential was taken at the vacuum level, around 4 eV above the CBM for ZnSe. This reduces the nonphysical increase of the confinement energy for the smallest seeds below 3 nm in diameter. Transition energies were calculated by adding the room temperature optical gap of bulk wurtzite ZnSe, set equal to 2.83 eV,[67] and neglecting the smaller hole confinement energies.

Conflict of Interest: The authors declare no competing financial interest.

Acknowledgment. The authors acknowledge financial support through the FP7 ERC starting grant NANO-ARCH (contract no. 240111).

Supporting Information Available: Chemicals and synthesis procedures; additional optical and electron microscopy data; Varshni fit parameters. This material is available free of charge *via* the Internet at http://pubs.acs.org.

REFERENCES AND NOTES

1. Hines, M. A.; Guyot-Sionnest, P. Bright UV-Blue Luminescent Colloidal ZnSe Nanocrystals. *J. Phys. Chem. B* **1998**, *102*, 3655–3657.
2. Reiss, P. ZnSe Based Colloidal Nanocrystals: Synthesis, Shape Control, Core/Shell, Alloy and Doped Systems. *New J. Chem.* **2007**, *31*, 1843–1852.
3. Kumar, P.; Singh, K. Wurtzite ZnSe Quantum dots: Synthesis, Characterization and PL Properties. *J. Optoelectron. Biomed. Mater.* **2009**, *1*, 59–69.
4. Pradhan, N.; Peng, X. G. Efficient and Color-Tunable Mn-Doped ZnSe Nanocrystal Emitters: Control of Optical Performance *via* Greener Synthetic Chemistry. *J. Am. Chem. Soc.* **2007**, *129*, 3339–3347.
5. Pradhan, N.; Battaglia, D. M.; Liu, Y. C.; Peng, X. G. Efficient, Stable, Small, and Water-Soluble Doped ZnSe Nanocrystal Emitters as Non-Cadmium Biomedical Labels. *Nano Lett.* **2007**, *7*, 312–317.
6. Chin, P. T. K.; Stouwdam, J. W.; Janssen, R. A. J. Highly Luminescent Ultranarrow Mn Doped ZnSe Nanowires. *Nano Lett.* **2009**, *9*, 745–750.
7. Cozzoli, P. D.; Manna, L.; Curri, M. L.; Kudera, S.; Giannini, C.; Striccoli, M.; Agostiano, A. Shape and Phase Control of Colloidal ZnSe Nanocrystals. *Chem. Mater.* **2005**, *17*, 1296–1306.
8. Song, K.-K.; Lee, S. Highly Luminescent (ZnSe)ZnS Core–Shell Quantum Dots for Blue to UV Emission: Synthesis and Characterization. *Curr. Appl. Phys.* **2001**, *1*, 169–173.
9. Nikesh, V. V.; Mahamuni, S. Highly Photoluminescent ZnSe/ZnS Quantum Dots. *Semicond. Sci. Technol.* **2001**, *16*, 687–690.
10. Lomascolo, M.; Creti, A.; Leo, G.; Vasanelli, L.; Manna, L. Exciton Relaxation Processes in Colloidal Core/Shell ZnSe/ZnS Nanocrystals. *Appl. Phys. Lett.* **2003**, *82*, 418–420.
11. Lad, A. D.; Mahamuni, S. Effect of ZnS Shell Formation on the Confined Energy Levels of ZnSe Quantum Dots. *Phys. Rev. B* **2008**, *78*, 125421.
12. Matylitsky, V. V.; Shavel, A.; Gaponik, N.; Eychmuller, A.; Wachtveitl, J. Ultrafast Interfacial Charge Carrier Dynamics in ZnSe and ZnSe/ZnS Core/Shell Nanoparticles: Influence of Shell Formation. *J. Phys. Chem. C* **2008**, *112*, 2703–2710.
13. Goswami, B.; Pal, S.; Sarkar, P. A Theoretical Study on the Electronic Structure of ZnSe/ZnS and ZnS/ZnSe Core/Shell Nanoparticles. *J. Phys. Chem. C* **2008**, *112*, 11630–11636.
14. Fang, Z.; Li, Y.; Zhang, H.; Zhong, X. H.; Zhu, L. Y. Facile Synthesis of Highly Luminescent UV-Blue-Emitting ZnSe/ZnS Core/Shell Nanocrystals in Aqueous Media. *J. Phys. Chem. C* **2009**, *113*, 14145–14150.
15. Zhu, D.; Jiang, X.; Zhao, C.; Sun, X.; Zhang, J.; Zhu, J.-J. Green Synthesis and Potential Application of Low-Toxic Mn: ZnSe/ZnS Core/Shell Luminescent Nanocrystals. *Chem. Commun.* **2010**, *46*, 5226–5228.
16. Rizzo, A.; Li, Y. Q.; Kudera, S.; Della Sala, F.; Zanella, M.; Parak, W. J.; Cingolani, R.; Manna, L.; Gigli, G. Blue Light Emitting Diodes Based on Fluorescent CdSe/ZnS Nanocrystals. *Appl. Phys. Lett.* **2007**, *90*, 051106.
17. Liu, F. C.; Cheng, T. L.; Shen, C. C.; Tseng, W. L.; Chiang, M. Y. Synthesis of Cysteine-Capped $Zn_xCd_{1-x}Se$ Alloyed Quantum Dots Emitting in the Blue-Green Spectral Range. *Langmuir* **2008**, *24*, 2162–2167.
18. Li, M. J.; Ouyang, J. Y.; Ratcliffe, C. I.; Pietri, L.; Wu, X. H.; Leek, D. M.; Moudrakovski, I.; Lin, Q.; Yang, B.; Yu, K. CdS Magic-Sized Nanocrystals Exhibiting Bright Band Gap Photoemission *via* Thermodynamically Driven Formation. *ACS Nano* **2009**, *3*, 3832–3838.
19. Wang, R. B.; Ratcliffe, C. I.; Wu, X. H.; Voznyy, O.; Tao, Y.; Yu, K. Magic-Sized Cd_3P_2 II–V Nanoparticles Exhibiting Band-gap Photoemission. *J. Phys. Chem. C* **2009**, *113*, 17979–17982.
20. Kim, M. R.; Park, S. Y.; Jang, D. J. Composition Variation and Thermal Treatment of $Zn_xCd_{1-x}S$ Alloy Nanoparticles To Exhibit Controlled and Efficient Luminescence. *J. Phys. Chem. C* **2010**, *114*, 6452–6457.
21. Chen, D. A.; Zhao, F.; Qi, H.; Rutherford, M.; Peng, X. G. Bright and Stable Purple/Blue Emitting CdS/ZnS Core/Shell Nanocrystals Grown by Thermal Cycling Using a Single-Source Precursor. *Chem. Mater.* **2010**, *22*, 1437–1444.
22. Lesnyak, V.; Dubavik, A.; Plotnikov, A.; Gaponik, N.; Eychmuller, A. One-Step Aqueous Synthesis of Blue-Emitting Glutathione-Capped $ZnSe_{1-x}Te_x$ Alloyed Nanocrystals. *Chem. Commun.* **2010**, *46*, 886–888.
23. Panda, S. K.; Hickey, S. G.; Waurisch, C.; Eychmuller, A. Gradated Alloyed CdZnSe Nanocrystals with High Luminescence Quantum Yields and Stability for Optoelectronic and Biological Applications. *J. Mater. Chem.* **2011**, *21*, 11550–11555.
24. Son, D. H.; Hughes, S. M.; Yin, Y. D.; Alivisatos, A. P. Cation Exchange Reactions in Ionic Nanocrystals. *Science* **2004**, *306*, 1009–1012.
25. Jain, P. K.; Amirav, L.; Aloni, S.; Alivisatos, A. P. Nanoheterostructure Cation Exchange: Anionic Framework Conservation. *J. Am. Chem. Soc.* **2010**, *132*, 9997–9999.
26. Robinson, R. D.; Sadtler, B.; Demchenko, D. O.; Erdonmez, C. K.; Wang, L. W.; Alivisatos, A. P. Spontaneous Superlattice Formation in Nanorods through Partial Cation Exchange. *Science* **2007**, *317*, 355–358.
27. Li, J. S.; Zhang, T. R.; Ge, H. P.; Yin, Y. D.; Zhong, W. W. Fluorescence Signal Amplification by Cation Exchange in Ionic Nanocrystals. *Angew. Chem., Int. Ed.* **2009**, *48*, 1588–1591.
28. Li, J. S.; Schachermeyer, S.; Wang, Y.; Yin, Y. D.; Zhong, W. W. Detection of MicroRNA by Fluorescence Amplification Based on Cation-Exchange in Nanocrystals. *Anal. Chem.* **2009**, *81*, 9723–9729.
29. Kelly, D.; Singh, A.; Barrett, C. A.; O'Sullivan, C.; Coughlan, C.; Laffir, F. R.; O'Dwyer, C.; Ryan, K. M. A Facile Spin-Cast Route for Cation Exchange of Multilayer Perpendicularly-Aligned Nanorod Assemblies. *Nanoscale* **2011**, *3*, 4580–4583.
30. Jain, P. K.; Beberwyck, B. J.; Fong, L. K.; Polking, M. J.; Alivisatos, A. P. Highly Luminescent Nanocrystals from Removal of Impurity Atoms Residual from Ion Exchange Synthesis. *Angew. Chem., Int. Ed.* **2012**, DOI: 10.1002/anie.201107452.
31. Li, H. B.; Zanella, M.; Genovese, A.; Povia, M.; Falqui, A.; Giannini, C.; Manna, L. Sequential Cation Exchange in Nanocrystals: Preservation of Crystal Phase and Formation of Metastable Phases. *Nano Lett.* **2011**, *11*, 4964–4970.
32. Carbone, L.; Nobile, C.; De Giorgi, M.; Sala, F. D.; Morello, G.; Pompa, P.; Hytch, M.; Snoeck, E.; Fiore, A.; Franchini, L.; *et al.* Synthesis and Micrometer-Scale Assembly of Colloidal CdSe/CdS Nanorods Prepared by a Seeded Growth Approach. *Nano Lett.* **2007**, *7*, 2942–2950.
33. Additional details on materials and methods are available in the Supporting Information.

34. Lin, S. L.; Pradhan, N.; Wang, Y. J.; Peng, X. G. High Quality ZnSe and ZnS Nanocrystals Formed by Activating Zinc Carboxylate Precursors. *Nano Lett.* **2004**, *4*, 2261–2264.
35. Luther, J. M.; Jain, P. K.; Ewers, T.; Alivisatos, A. P. Localized Surface Plasmon Resonances Arising from Free Carriers in Doped Quantum Dots. *Nat. Mater.* **2011**, *10*, 361–366.
36. Dorfs, D.; Hartling, T.; Miszta, K.; Bigall, N. C.; Kim, M. R.; Genovese, A.; Falqui, A.; Povia, M.; Manna, L. Reversible Tunability of the Near-Infrared Valence Band Plasmon Resonance in $Cu_{2-x}Se$ Nanocrystals. *J. Am. Chem. Soc.* **2011**, *133*, 11175–11180.
37. Kriegel, I.; Jiang, C. Y.; Rodríguez-Fernández, J.; Schaller, R. D.; Talapin, D. V.; Da Como, E.; Feldmann, J. Tuning the Excitonic and Plasmonic Properties of Copper Chalcogenide Nanocrystals *J. Am. Chem. Soc.* **2011**, *134*, 1583−1590.
38. Zhao, Y.; Burda, C. Development of Plasmonic Semiconductor Nanomaterials with Copper Chalcogenides for a Future with Sustainable Energy Materials *Energy Environ. Sci.* **2012**, *5*, 5564−5576.
39. Odonnell, K. P.; Chen, X. Temperature-Dependence of Semiconductor Band-Gaps. *Appl. Phys. Lett.* **1991**, *58*, 2924–2926.
40. Dawood, F.; Schaak, R. E. ZnO-Templated Synthesis of Wurtzite-Type ZnS and ZnSe Nanoparticles. *J. Am. Chem. Soc.* **2009**, *131*, 424–425.
41. Joo, J.; Na, H. B.; Yu, T.; Yu, J. H.; Kim, Y. W.; Wu, F. X.; Zhang, J. Z.; Hyeon, T. Generalized and Facile Synthesis of Semiconducting Metal Sulfide Nanocrystals. *J. Am. Chem. Soc.* **2003**, *125*, 11100–11105.
42. Reiss, P.; Protiere, M.; Li, L. Core/Shell Semiconductor Nanocrystals. *Small* **2009**, *5*, 154–168.
43. Zhao, Y. W.; Zhang, Y.; Zhu, H.; Hadjipianayis, G. C.; Xiao, J. Q. Low-Temperature Synthesis of Hexagonal (Wurtzite) ZnS Nanocrystals. *J. Am. Chem. Soc.* **2004**, *126*, 6874–6875.
44. Banerjee, I. A.; Yu, L. T.; Matsui, H. Room-Temperature Wurtzite ZnS Nanocrystal Growth on Zn Finger-like Peptide Nanotubes by Controlling Their Unfolding Peptide Structures. *J. Am. Chem. Soc.* **2005**, *127*, 16002–16003.
45. Chen, H.-S.; Lo, B.; Hwang, J.-Y.; Chang, G.-Y.; Chen, C.-M.; Tasi, S.-J.; Wang, S.-J. J. Colloidal ZnSe, ZnSe/ZnS, and ZnSe/ZnSeS Quantum Dots Synthesized from ZnO. *J. Phys. Chem. B* **2004**, *108*, 17119–17123.
46. Wu, Q.; Cao, H.; Zhang, S.; Zhang, X.; Rabinovich, D. Generation and Optical Properties of Monodisperse Wurtzite-Type ZnS Microspheres. *Inorg. Chem.* **2006**, *45*, 7316–7322.
47. Xi, B.; Xiong, S.; Xu, D.; Li, J.; Zhou, H.; Pan, J.; Li, J.; Qian, Y. Tetraethylenepentamine-Directed Controllable Synthesis of Wurtzite ZnSe Nanostructures with Tunable Morphology. *Chem.—Eur. J.* **2008**, *14*, 9786–9791.
48. Yu, J. H.; Joo, J.; Park, H. M.; Baik, S. I.; Kim, Y. W.; Kim, S. C.; Hyeon, T. Synthesis of Quantum-Sized Cubic ZnS Nanorods by the Oriented Attachment Mechanism. *J. Am. Chem. Soc.* **2005**, *127*, 5662–5670.
49. Deng, Z.; Yan, H.; Liu, Y. Controlled Colloidal Growth of Ultrathin Single-Crystal ZnS Nanowires with a Magic-Size Diameter. *Angew. Chem., Int. Ed.* **2010**, *49*, 8695–8698.
50. Hytch, M. J.; Snoeck, E.; Kilaas, R. Quantitative Measurement of Displacement and Strain Fields from HREM Micrographs. *Ultramicroscopy* **1998**, *74*, 131–146.
51. Galindo, P. L.; Kret, S.; Sanchez, A. M.; Laval, J.-Y.; Yanez, A.; Pizarro, J.; Guerrero, E.; Ben, T.; Molina, S. I. The Peak Pairs Algorithm for Strain Mapping from HRTEM Images. *Ultramicroscopy* **2007**, *107*, 1186–1193.
52. Dong, B.; Cao, L.; Su, G.; Liu, W. Facile Synthesis of Highly Luminescent UV-Blue Emitting ZnSe/ZnS Core/Shell Quantum Dots by a Two-Step Method. *Chem. Commun.* **2010**, *46*, 7331–7333.
53. Aboulaich, A.; Geszke, M.; Balan, L.; Ghanbaja, J.; Medjahdi, G.; Schneider, R. I. Water-Based Route to Colloidal Mn-Doped ZnSe and Core/Shell ZnSe/ZnS Quantum Dots. *Inorg. Chem.* **2010**, *49*, 10940–10948.
54. Smith, A. M.; Nie, S. Bright and Compact Alloyed Quantum Dots with Broadly Tunable Near-Infrared Absorption and Fluorescence Spectra through Mercury Cation Exchange. *J. Am. Chem. Soc.* **2010**, *133*, 24–26.
55. Pietryga, J. M.; Werder, D. J.; Williams, D. J.; Casson, J. L.; Schaller, R. D.; Klimov, V. I.; Hollingsworth, J. A. Utilizing the Lability of Lead Selenide To Produce Heterostructured Nanocrystals with Bright, Stable Infrared Emission. *J. Am. Chem. Soc.* **2008**, *130*, 4879–4885.
56. Sitt, A.; Sala, F. D.; Menagen, G.; Banin, U. Multiexciton Engineering in Seeded Core/Shell Nanorods: Transfer from Type-I to Quasi-type-II Regimes. *Nano Lett.* **2009**, *9*, 3470–3476.
57. Northrup, J. E.; Ihm, J.; Cohen, M. L. Electronic Structure of Zinc-Blende-Wurtzite Interfaces: ZnS−ZnS (111−0001) and ZnSe-ZnSe (111−0001). *Phys. Rev. B* **1980**, *22*, 2060–2065.
58. Smith, A. M.; Mohs, A. M.; Nie, S. Tuning the Optical and Electronic Properties of Colloidal Nanocrystals by Lattice Strain. *Nat. Nanotechnol.* **2009**, *4*, 56–63.
59. Li, Y.-H.; Gong, X. G.; Wei, S.-H. *Ab Initio* All-Electron Calculation of Absolute Volume Deformation Potentials of IV−IV, III−V, and II−VI Semiconductors: The Chemical Trends. *Phys. Rev. B* **2006**, *73*, 245206.
60. Morello, G.; Della Sala, F.; Carbone, L.; Manna, L.; Maruccio, G.; Cingolani, R.; De Giorgi, M. Intrinsic Optical Nonlinearity in Colloidal Seeded Grown CdSe/CdS Nanostructures: Photoinduced Screening of the Internal Electric Field. *Phys. Rev. B* **2008**, *78*, 195313.
61. Rainò, G.; Stoferle, T.; Moreels, I.; Gomes, R.; Kamal, J. S.; Hens, Z.; Mahrt, R. F. Probing the Wave Function Delocalization in CdSe/CdS Dot-in-Rod Nanocrystals by Time- and Temperature-Resolved Spectroscopy. *ACS Nano* **2011**, *5*, 4031–4036.
62. She, C.; Demortière, A.; Shevchenko, E. V.; Pelton, M. Using Shape To Control Photoluminescence from CdSe/CdS Core/Shell Nanorods. *J. Phys. Chem. Lett.* **2011**, *2*, 1469–1475..
63. van Driel, A. F.; Allan, G.; Delerue, C.; Lodahl, P.; Vos, W. L.; Vanmaekelbergh, D. Frequency-Dependent Spontaneous Emission Rate from CdSe and CdTe Nanocrystals: Influence of Dark States. *Phys. Rev. Lett.* **2005**, *95*, 236804.
64. Yu, P. Y.; Cardona, M. *Fundamentals of Semiconductors: Physics and Materials Properties*; Springer: Berlin, 2010.
65. Deng, Z.; Lie, F. L.; Shen, S.; Ghosh, I.; Mansuripur, M.; Muscat, A. J. Water-Based Route to Ligand-Selective Synthesis of ZnSe and Cd-Doped ZnSe Quantum Dots with Tunable Ultraviolet A to Blue Photoluminescence. *Langmuir* **2008**, *25*, 434–442.
66. Cardona, M. Band Parameters of Semiconductors with Zincblende, Wurtzite, and Germanium Structure. *J. Phys. Chem. Solids* **1963**, *24*, 1543–1555.
67. Bhargava, R. *Properties of Wide Bandgap II−VI Semiconductors*; The Institution of Engineering and Technology, **1997**.